Chemistry of Materials

This document is confidential and is proprietary to the American Chemical Society and its authors. Do not copy or disclose without written permission. If you have received this item in error, notify the sender and delete all copies.

Porous Ion Exchange Polymer Matrix for Ultra-Small Au Nanoparticles-Decorated Carbon Nanotube Chemiresistors

Journal:	Chemistry of Materials
Manuscript ID	cm-2019-00504z.R2
Manuscript Type:	Article
Date Submitted by the Author:	n/a
Complete List of Authors:	Koo, Won-Tae; Korea Advanced Institute of Science and Technology, Dept. of Materials Science and Engineering Kim, Yoonseob; Massachusetts Institute of Technology, Chemistry Savagatrup, Suchol; Massachusetts Institute of Technology, Chemistry Yoon, Bora; Massachusetts Institute of Technology, Chemistry Jeon, Intak; Massachusetts Institute of Technology, Chemistry Choi, Seon-Jin; Massachusetts Institute of Technology, Chemistry Kim, Il-Doo; Korea Advanced Institute of Science and Technology, Dept. of Materials Science and Engineering; Swager, Timothy; Massachusetts Institute of Technology, Chemistry

SCHOLARONE™ Manuscripts

60

Porous Ion Exchange Polymer Matrix for Ultra-Small Au Nanoparticles-Decorated Carbon Nanotube Chemiresistors

Won-Tae Koo, $^{\dagger, \pm, \S}$ Yoonseob Kim, $^{\S, \perp}$ Suchol Savagatrup, $^{\S, \perp}$ Bora Yoon, $^{\perp, \P}$ Intak Jeon, $^{\S, \perp}$ Seon-Jin Choi, § Il-Doo Kim, $^{\dagger, \pm, *}$ and Timothy M. Swager $^{\S, \perp, *}$

[†]Department of Materials Science and Engineering, Korea Advanced Institute of Science and Technology (KAIST), Daejeon 34141, Republic of Korea

‡Advanced Nanosensor Research Center, KAIST Institute for Nanocentury, Daejeon 34141, Republic of Korea

§Department of Chemistry and ¹Institute for Soldier Nanotechnologies, Massachusetts Institute of Technology, Cambridge, Massachusetts 02139, United States

[¶]Optical and Electromagnetic Materials Team, U.S. Army Combat Capabilities Development Command-Soldier Center (CCDC-Soldier Center), Natick, Massachusetts 01760, United States

KEYWORDS. Carbon monoxide, porous ion exchange polymers, Au nanoparticles, carbon nanotubes, sensors, chemical field-effect transistors.

ABSTRACT: Single-walled carbon nanotubes (SWCNTs) are recognized as versatile materials for the formation of chemiresistive sensors. However, imparting high sensitivity and selectivity to SWCNTs remains a major challenge. Herein, we report a new sensory system that interfaces SWCNTs and catalytic metal nanoparticles (NPs) in a film of a porous ion exchange polymer to produce sensitive and selective sensors. The porous polymer films are based on imidazolium-functionalized triptycene polyether sulfone and the environment created by this polymer results in the formation of ultrasmall (< 5 nm) Au NPs. The polymer serves to suppress the growth of Au NPs while maintaining gas transport. The size control promotes strong interactions between Au NPs and carbon monoxide (CO) and this composition produces a robust, sensitive, and selective CO chemiresistive sensor. We further demonstrate that modulation of a gate voltage in chemical field-effect transistor sensing devices enhances the performance by promoting the activity of Au NPs. Sensors display an increase of CO sensitivity at room temperature in air under the negative gate voltage. Our results demonstrate that the combination of porous ion exchange matrix, nanoparticles, and gate voltage modulated chemiresistors can be synergistically tuned to create sensitive and selective sensors for target analytes.

INTRODUCTION

Chemical sensors can be used to protect human beings from toxic and explosive chemicals,1 to monitor air and food quality,2 and to provide an early diagnosis of disease.3 Chemiresistors are particularly attractive as a result of their electrical transduction signals and facile integration with other electronic devices.4 Although metal oxide-based chemiresistors are commercially available, their low selectivity and high operating temperatures limit their utility.^{5,6} Chemiresistors that operate at ambient temperatures are attractive as a result of their low power requirements and ability to differentiate chemicals based on inherent reactivity and molecular recognition. Singlewalled carbon nanotubes (SWCNTs) are one of the more attractive chemiresistive sensor elements because they can be chemically functionalized to incorporate catalysts or selectors, operate at ambient temperature, and have tunable semiconducting electrical properties.7 The

combination of SWCNTs and metal nanoparticles (NPs) recognized as presenting been previously opportunities for gas sensing, 8-10 by leveraging the catalytic properties of metal NPs that are a few nanometers in size.11,12 However, despite successful demonstrations of metal NPs-functionalized SWCNT chemiresistors, the uniform fabrication of ultra-small metal NPs on SWCNTs has been achieved by electrochemical deposition and physical vapor deposition methods, which can complicate the fabrication process.^{13,14} A pressing problem with existing schemes is that van der Waals attraction causes aggregation of ultra-small metal NPs,15,16 which degrades their activity. As a result, we have targeted methods that prevent NP aggregation/fusion and allow for facile fabrication.

We report herein the facile and uniform decoration of ultra-small metal NPs on SWCNTs *via* ion exchange through a porous ion exchange polymer matrix.

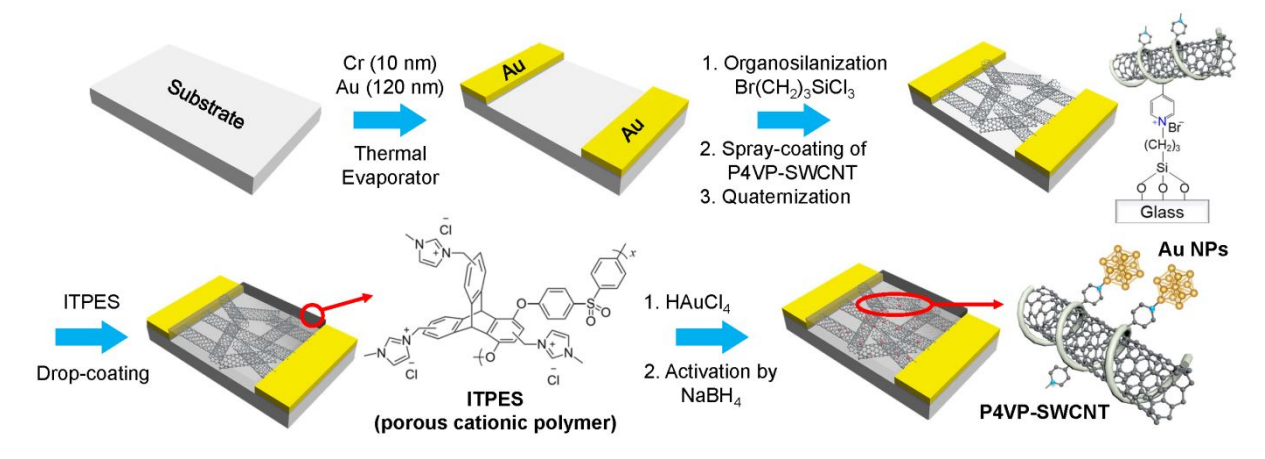


Figure 1. Schematic illustration of the preparation of P4VP-SWCNT/Au@ITPES.

The introduction of the porous ion exchange polymer matrix with SWCNTs-based sensors facilitates a uniform formation of ultra-small Au NPs onto the sensing layer. Specifically, the ion conducting and porous polymer film allows the transport of ionic metal precursors with complementary charge, while maintaining high gas diffusion within the sensing layer.^{17,18} The rigid nanoporous polymer structure additionally suppresses Oswald ripening of metal NPs during the activation of metal precursors,19 creating well-dispersed metal NPs of only a few nanometers in dimension. In this investigation, we synthesized ultra-small (~ 4.6 nm) Au NPs that interact with SWCNTs in a porous anion exchange polymer matrix. Au NPs are well-known room temperature catalysts for the oxidation of CO that is activated by coordination to Au NPs. 20-22 Inspired by this exceptional high CO activation by Au NPs, we have developed highly sensitive and selective CO detectors by using a porous ion exchange matrix to create Au NPs functionalized SWCNT conductive networks. The unique material characteristics and sensing properties were verified by experimental demonstrations and theoretical calculations. In addition, we report that a chemical field-effect transistor (Chem-FET) sensing scheme delivers enhanced CO sensing characteristics at room temperature in air, by electrical tuning of Au catalysis.

RESULTS AND DISCUSSION

Figure 1 illustrates the fabrication of Au NPsfunctionalized SWCNT-based chemiresistors using a porous ion exchange polymer matrix. Spray-coating of poly(4-vinylpyridine) (P4VP) wrapped SWCNT (P4VP-SWCNT) composites onto alkyl halide functional glass surfaces with Au electrode arrays results in covalent anchoring via quaternization reactions (Details in Supporting Information). This covalent linking of P4VP-SWCNT composites has proved very effective to produce high stability SWCNT-based sensors.²³ After the deposition of P4VP-SWCNT, imidazolium-functionalized triptycene polyether sulfone (ITPES) ion exchange material is dropcast as an overcoat. ITPES was synthesized by the chloromethylation of triptycene polyether sulfone (TPES)¹⁷ and subsequent quaternization reaction (Figure S1, see details in the Supporting Information). The structures of

the synthetic intermediates and ITPES were confirmed by the ¹H-NMR analysis (Figure S₂ and S₃). ITPES derives its porosity from the free volume promoting properties of triptycene,24 and NP anion precursors are readily incorporated as a result of the positively charged imidazolium groups.¹⁷ The P₄VP-SWCNT films before and after ITPES deposition showed similar morphologies (Figure S4), and the thickness of ITPES film was verified to be ca. 170 nm by the surface profilometer analysis (Figure S₅). An aqueous solution (5.0 µl, 2.94 mM) of HAuCl₄ is then deposited over a total area of ~ 10 mm² and AuCl₄- ions are incorporated. The acidity of the solution promotes protonation of the pyridine groups of P4VP-SWCNT network and facilitates intimate contact with the NP precursor. The AuCl₄ ions are converted to Au NPs by sodium borohydride (NaBH₄) reduction and we expect that the pyridine groups continue to promote proximate localization of the NPs via coordination. The growth of Au NPs is suppressed by the porous ITPES matrix and the Au NPs are limited to a few nanometers in size within P4VP-SWCNT sensing matrix.

We confirmed the size and distribution of the Au NPs via transmission electron microscopy (TEM) analysis. The Au NPs are well-dispersed on ITPES-coated P4VP-SWCNT (P4VP-SWCNT/ITPES) (Figure 2a), with the average size of 4.64 ± 0.82 nm (N = 147) (**Figure 2b**). Hereafter, Au NP decorated P4VP-SWCNT/ITPES is denoted as P4VP-SWCNT/Au@ITPES. The high-resolution TEM (HRTEM) image further revealed that ultra-small Au NPs were attached to SWCNT bundles (Figure 2c). Control samples prepared without the ITPES overcoat reveal that larger (> 20 nm) Au NPs were agglomerates on the surface of P4VP-SWCNT (**Figure S6**). In addition, energy dispersive X-ray spectroscopy (EDS) elemental mapping analysis using scanning electron microscopy (SEM) confirmed C, N, S, and Au in P4VP-SWCNT/Au@ITPES (Figure S7). Hence, we conclude that the combination of ITPES and P4VP-SWCNT produces Au NP functionalized SWCNTs.

To further verify the penetration of the solution of Au precursors through the porous ion exchange polymer and the decoration of Au NPs on P4VP-SWCNT, we performed attenuated total reflection-Fourier-transform infrared spectroscopy (ATR-FTIR) analysis. The ATR-FTIR spectra

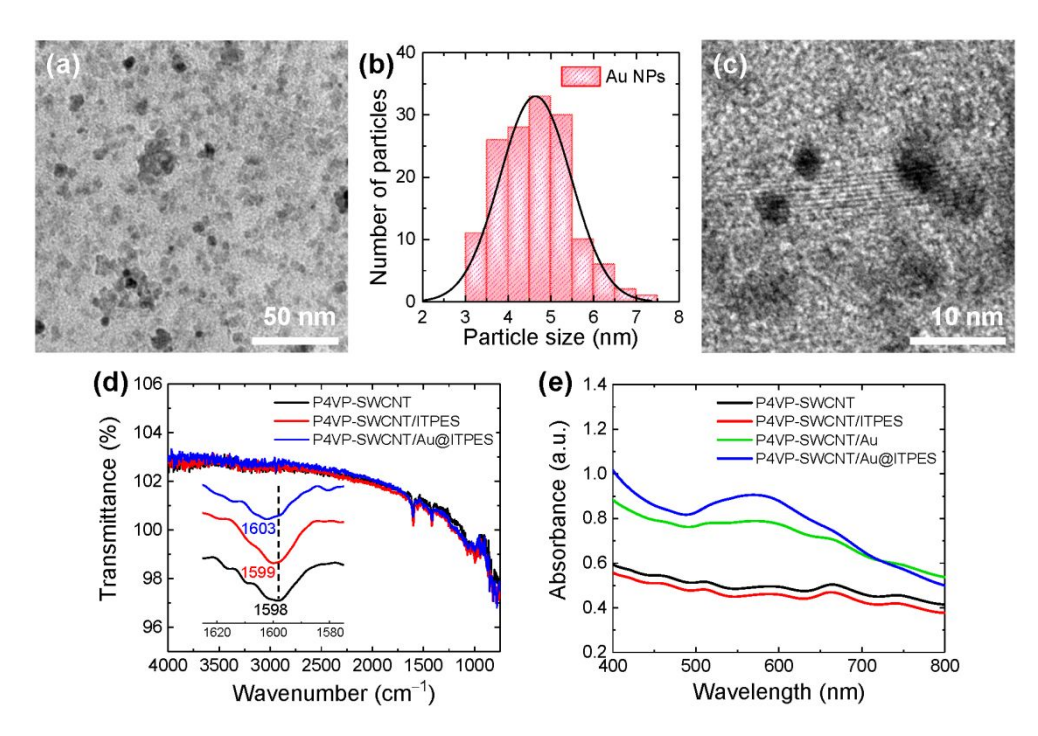


Figure 2. Characterization of the Au NPs in P4VP-SWCNT/ITPES. (a) TEM image of P4VP-SWCNT/Au@ITPES, (b) Size distribution of Au NPs, (c) HR-TEM image of P4VP-SWCNT/Au@ITPES, (d) ATR-FTIR spectra of the samples, and (e) UV-Vis spectra of the samples.

of P4VP-SWCNT/Au@ITPES exhibit the shift of C=N stretching band (from 1598 to 1603 cm⁻¹) for the pyridine in P4VP (**Figure 2d**). This peak shift to higher wavenumber is consistent with coordination bonding between transition metal NPs and pyridine group.25 This shift was also observed in the ATR-FTIR spectra of the control sample fabricated without ITPES (P4VP-SWCNT/Au) (Figure S8). In addition, ultraviolet-visible (UV-Vis) spectra also display the features expected for the Au NPs in the composite films (Figure 2e). Specifically, the UV-Vis spectrum of pristine P4VP-SWCNT film show a distinct absorbance pattern of unbundled SWCNTs.23 After the deposition of ITPES, there is no significant difference for P4VP-SWCNT/IPTES as a result of its thinness (~ 170 nm) and lack of absorption transitions in the visible range. In contrast, the UV-Vis spectrum of P₄VP-SWCNT/Au@ITPES exhibit an intense localized surface plasmon resonance (LSPR) associated with Au NPs from 500-650 nm.²⁶ The LSPR absorption spectrum is significantly reduced for P4VP-SWCNT/Au prepared without ITPES layer as a result of the larger particle sizes. In addition, although matrix materials typically cause a red shift of LSPR peak by increasing the dielectric constant of Au surrounding, 20,27 the LSPR peak expected for the Au NPs is blue-shifted from 579 nm for P4VP-SWCNT/Au to 568 nm for P4VP-SWCNT/Au@ITPES. The blue shift in the LSPR of Au is an indication of the size control, 20,28 and the free volume (porosity) of the ITPES matrix.

We also performed X-ray photoelectron spectroscopy (XPS) analysis to further confirm the nature of the Au NPs in P4VP-SWCNT/Au@ITPES composition (**Figure 3** and **Figure S9**). The high-resolution spectra of the samples in the vicinity of C is are deconvoluted into three peaks at 284.5, 285.5, and 286.5 eV (**Figure 3a**), which are

corresponded to C–C, C–N, and C–O bondings.²⁹ The C–C bonding peak originates from SWCNT, P₄VP, and ITPES; the C–N bonding is related to the N in P₄VP and imidazolium; and, the C–O peak is ascribed to the O in ITPES. The N is peaks in XPS analysis show the characteristic peaks of pyridine N at 398.2 eV, imidazole N at 399.5 eV, and imidazole N⁺ at 401.0 eV.^{29,30} The XPS spectra of S 2p exhibit the sulfone groups in ITPES with the specific peaks at 168.5 eV for 2p_{3/2} and 169.7 eV for 2p_{1/2}.³¹ Therefore, the XPS spectra of C is, N is, and S 2p confirm the that P₄VP-SWCNT and ITPES are intact as expected,

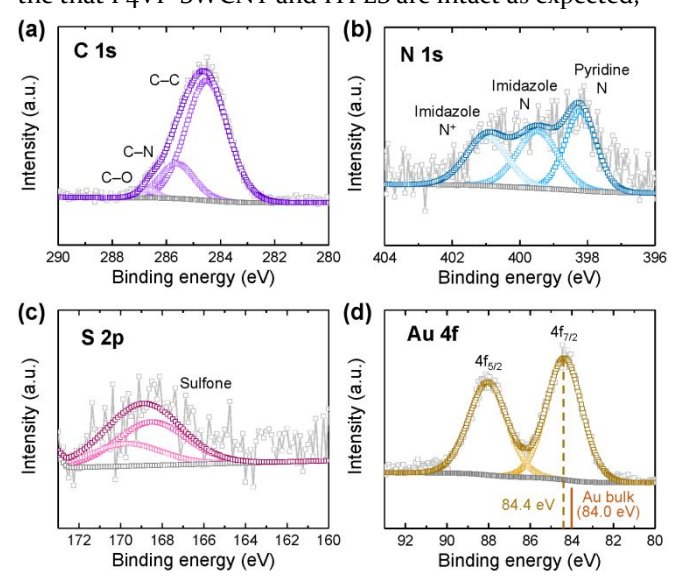


Figure 3. XPS spectra of P4VP-SWCNT/Au@ITPES. High-resolution spectra in the vicinity of (a) C is, (b) N is, (c) S 2p, and (d) Au 4f, respectively.

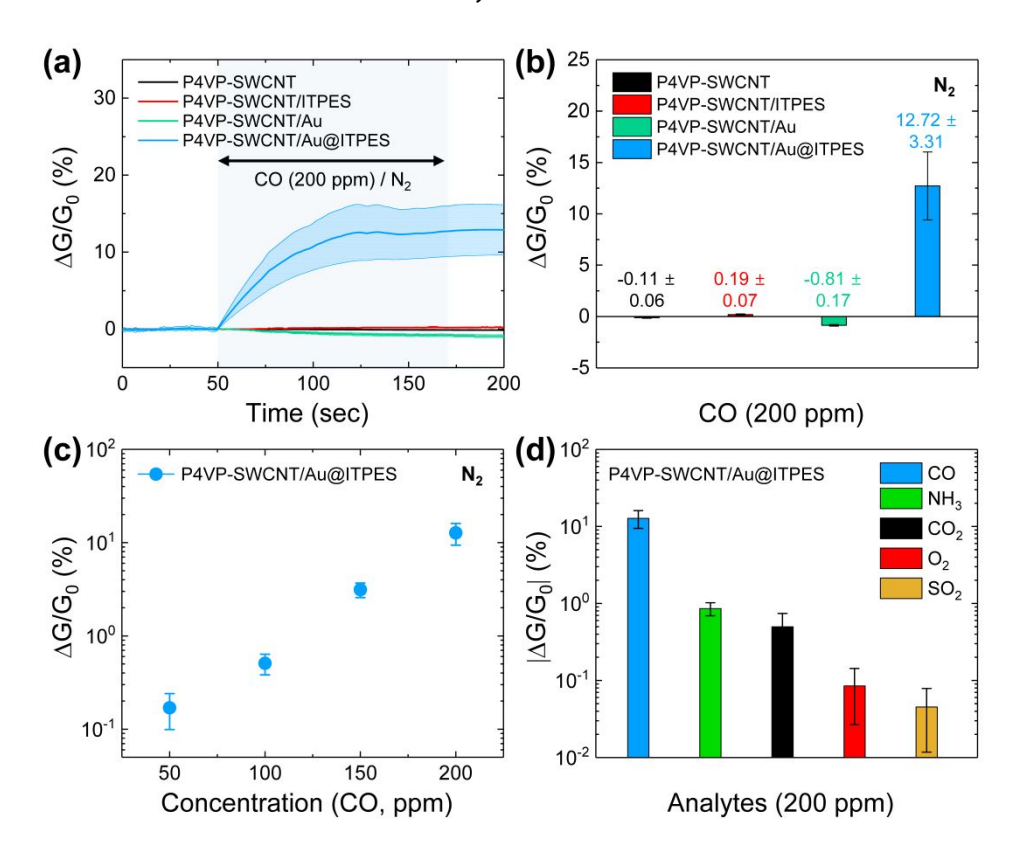


Figure 4. Sensing characteristics of P4VP-SWCNT, P4VP-SWCNT/ITPES, P4VP-SWCNT/Au, and P4VP-SWCNT/Au@ITPES at room temperature in N_2 atmospheres ($N \ge 4$ sensors). (a) Conductance traces and (b) responses of the sensors to 2 min exposure to 200 ppm of CO. The shaded area indicates the standard deviation. (c) Responses vs. CO concentrations for P4VP-SWCNT/Au@ITPES based sensors. (d) Responses of P4VP-SWCNT/Au@ITPES to 200 ppm of other interfering gases (NH₃, CO₂, O₂, and SO₂) in N₂.

in the samples. In addition, the high-resolution XPS spectra of Au 4f exhibit two major peaks at 84.4 eV for $4f_{7/2}$ and 88.0 eV for $4f_{5/2}$. Interestingly, the binding energy for Au $4f_{7/2}$ is shifted to higher energy (+0.4 eV) compared with that of bulk Au (84.0 eV). This shift to higher binding energy is characteristic of small Au NPs wherein the electrons are more strongly bound to the Au nuclei as a result of quantum confinement.^{32,33} In contrast, the control sample without ITPES (P4VP-SWCNT/Au) exhibits the split of Au $4f_{7/2}$ peak into Au clusters and Au bulk peaks (**Figure S10**), indicating the agglomeration of Au NPs. The XPS results demonstrate the critical role of the porous ion exchange polymer (ITPES) to stabilize ultra-small discrete Au NPs on P4VP-SWCNT.

In developing CO P₄VPsensors using SWCNT/Au@ITPES, we considered that Au NPs, in addition to their role in transduction, could also provide an impediment to gas diffusion in ITPES. As a result, we varied the Au NPs loading in P4VP-SWCNT/ITPES by changing the concentration of Au precursors (**Figure S11**). To optimize the conditions, we investigated the CO sensing properties of P₄VP-SWCNT/Au@ITPES, as well as control samples; without porous polymer/Au (P4VP-SWCNT), without Au (P4VP-SWCNT/ITPES), and without porous polymer (P4VP-SWCNT/Au). The sensing tests were initially carried out at room temperature in N2, and as shown in Figure 4a. The P4VP-SWCNT/Au@ITPES exhibits a significant increase in net conductance of 12.72% with a 2 min exposure to 200 ppm CO, whereas the other control samples showed negligible responses under the

same conditions. In contrast, P4VP-SWCNT/Au displays a small decrease in conductance. It is also noted that P4VP-SWCNT/Au sensors showed irreversible dosimetric responses to CO, consistent with the formation of a strong static complex with the larger Au NPs. Dosimetric sensors offer a different type of information than recoverable sensors, especially for total exposure rather than instantaneous per event. Similar effects have also been observed in other studies on SWCNT-based CO sensors. 8,34 The recovery of CNT-based sensors can be improved by applying high temperature or UV light,8,35 but these procedures will complicate the overall sensing devices as compared to room temperature operating sensors. The P4VP-SWCNT/Au@ITPES shows 15.7-fold higher response $(\Delta G/G_0 = 12.72\%)$ when compared to P4VP-SWCNT/Au $(|\Delta G/G_0| = 0.81\%)$ (**Figure 4b**) upon exposure to 200 ppm CO for 2 min in N2, demonstrating the critical effect of the ITPES-assisted size control/stabilization of the Au NPs on CO sensing. The P4VP-SWCNT/Au@ITPES also showed a noticeable response (0.17%) to 50 ppm of CO (Figure 4c and Figure S12a). This is significantly below Occupational Safety and Health Administration (OSHA) ceiling (5 min) CO exposure limit 200 ppm.36 In addition, the sensor signals were remained relatively constant for 30 min after the initial exposures (Figure S12b). Furthermore, the sensors exhibit a relatively fast response time (57 sec to 200 ppm of CO) (Figure S12c), and high CO response compared to the response to other generally more reactive interfering gases (NH₃, CO₂, O₂, and SO₂) at the same concentrations in N₂ (Figure 4d).

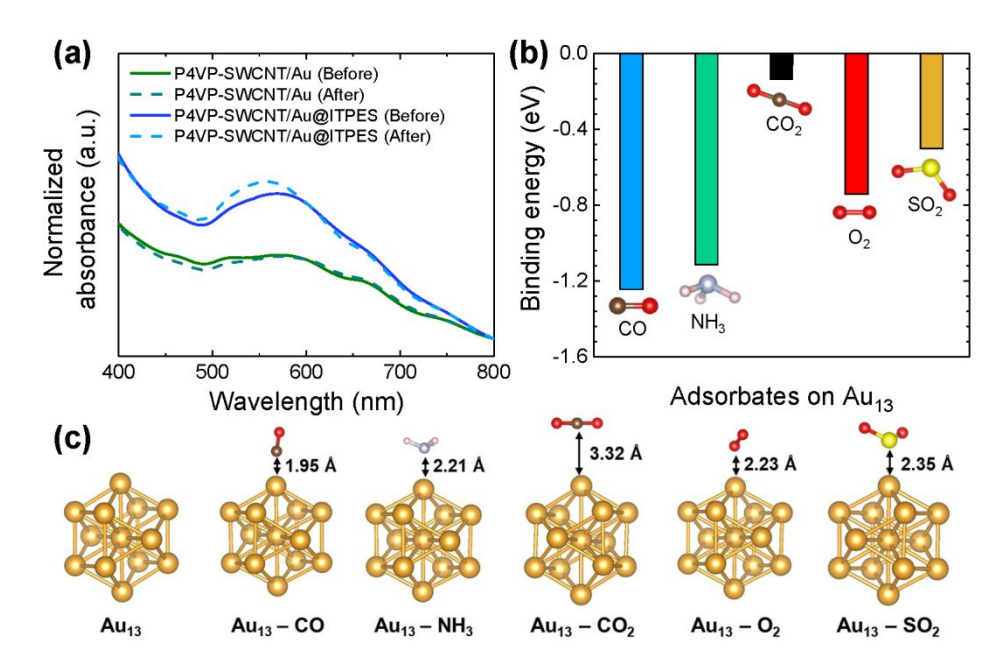


Figure 5. Proposed sensing mechanism and selectivity of Au NPs toward CO. (a) Ex-situ UV-Vis spectra of the samples before and after exposure of 200 ppm of CO for 5 min. DFT calculation of the adsorption of analytes (CO, NH₃, CO₂, O₂, and SO₂) on Au₁₃: (b) Calculated adsorption energy and (c) calculated optimum geometry for each adsorption.

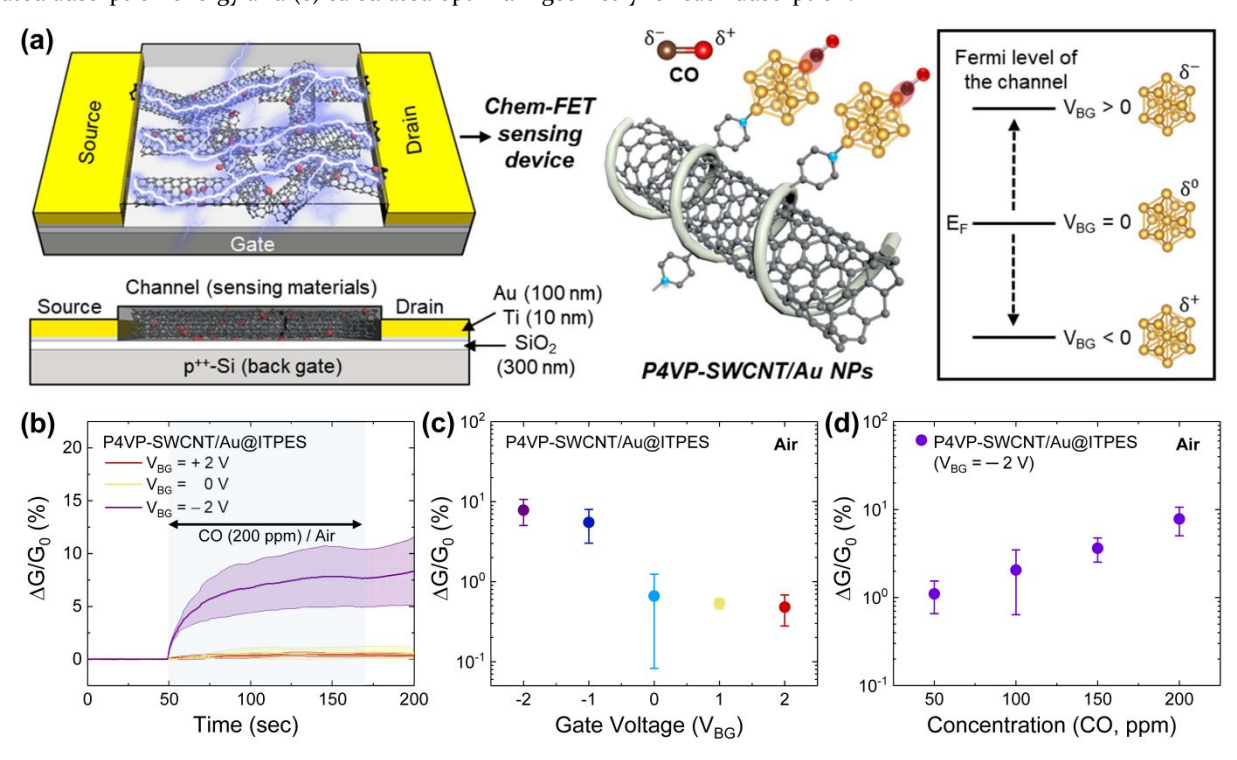


Figure 6. Characterization of Chem-FET sensors in air. (a) Schematic illustration of Chem-FET sensors using P4VP-SWCNT/Au@ITPES as a channel layer, and the sensing mechanism of the Chem-FET sensors. (b–d) Sensing characteristics of the Chem-FET sensors to 2 min exposure to CO at room temperature in air ($N \ge 4$ sensors). The shaded area indicates the standard deviation. (b) Chemiresistive traces at + 2, 0, and – 2 V_{BG} to 200 ppm of CO, (c) responses to 200 ppm of CO as a function of the gate voltage, (d) responses to 50–200 ppm of CO under –2 V_{BG}.

To support our hypothesis that ultra-small Au NPs derived from porous polymer matrix enhance CO sensing properties of SWCNTs, we carried out ex-situ UV-Vis analysis. It has been previously reported that the unsaturated coordination sites on the surface of Au NPs can facilitate CO adsorption.^{37,38} The adsorbed CO molecules on these sites strongly interact with the Au atoms with sigma donation ($\sigma_{CO} \rightarrow d_{Au}$) and back-donation

 $(d_{Au} \rightarrow \pi_{CO})$.^{38,39} This results in a shift of the Au NP LSPR peaks with CO adsorption.⁴⁰ Specifically, we observed a LSPR shift from 568 nm to 559 nm in P4VP-SWCNT/Au@ITPES after the exposure of CO 200 ppm for 5 min while that of P4VP-SWCNT/Au optical spectra remained unchanged after CO exposure (**Figure 5a**). This result confirms that more CO molecules adsorb and change the electronic states of the Au NPs in P4VP-

SWCNT/Au@ITPES. The blue shift of the LSPR peak also is consistent with increase of free electrons in Au NPs, 21 as predicted by the Bylhoder model 41 wherein σ_{CO} electron donation to d_{Au} dominates the interaction.

Density functional theory (DFT) was employed to investigate the origin of the selectivity of the sensors. To simplify the DFT calculations, we used cuboctahedral Au₁₃ as an adsorbent in the calculations, which is the smallest Au cluster with a face-centered cubic structure. 42 Pristine P4VP-SWCNT exhibits no response to CO, and as a result the P₄VP wrapping of the SWCNT doesn't appear to have a direct effect on the CO sensitivity and therefore was not taken into account in the DFT calculations. The calculated binding energy (-1.25 eV) of CO on Au,3 is the strongest among the adsorbates considered (CO, NH₂, CO₂, O₂, and SO₃) (**Figure 5b**), which again suggests that the Au NPs are responsible for the high CO selectivity in these SWCNTsbased sensors. We attributed the opposing trend in the calculated binding energy and the chemiresistive CO2 sensing response (Figure 4d) to the effect of imidazolium groups in ITPES. Imidazolium groups have an affinity to bind with CO2 by forming carbonates.43 The calculated optimum geometry of Au₁₃-CO shows that the negative potential on the carbon ($C^{\delta-}$) of CO strongly interacts with Au₁₃ (**Figure 5c**). This sensing mechanism is also confirmed by the sensing measurements in the ambient atmosphere. In this case oxygen molecules in air can also adsorb on the Au NPs, and thereby block the active sites. The competitive adsorption of CO and O₂ on Au NPs decreases the amount of adsorbed CO molecules on Au NPs. Therefore, the sensors exhibit lower CO responses in air as compared to N₂ atmosphere (**Figure S13**).

To improve the sensing properties in air, we have created Chem-FET based CO sensors with SWCNT/Au@ITPES as a channel layer. The sensing materials were fabricated on the FET substrates having a heavily p-doped Si (p++-Si) back gate by using the same process as the chemiresistor fabrication (Figure 6a and experimental details in Supporting Information). The electrical properties of the channel layer can then be tuned by applying a back gate voltage (V_{BG}),44 which facilitates the CO adsorption on Au NPs in air atmosphere. In brief, because the Fermi level (E_F) of the channel is decreased when negative V_{BG} is applied, the sensing layer becomes electron-deficient. Therefore, the adsorption of the strongly donating ($C^{\delta-}$) CO is enhanced to the more electron-deficient Au (Au $^{\delta+}$). 45,46 We have also confirmed that the semiconducting nature of P4VP-SWCNT is not responsible for the voltage-activated sensitivity (Figure S14). The Chem-FET sensors exhibit improved CO sensing properties from 0.66% at o V to 7.83% in ambient air under an applied negative V_{BG} (-2 V) (Figure 6b and 6c). The Chem-FET sensors also showed dosimetric sensing behaviors. Although the Chem-FET sensors was not recovered after CO exposure, they showed conductance changes even to repeated exposure to 200 ppm CO (Figure **S15a**). The standard deviation of the sensors was increased as repeating CO exposures, which is one of limitations of CNT-based chemiresistors because CNT mixture is composed of diverse CNTs having different lengths, diameters, and electrical properties. The Chem-FET

sensors have a noticeable response (1.10%) to the 50 ppm OSHA transitional time weighted average (TWA, 8 h) exposure limit for CO (Figure 6d and Figure S15b).36 Additionally, the Chem-FET sensors exhibited a comparable response (7.05%) at 200 ppm CO in high humidity atmospheres (85% RH at 22 °C) (Figure S16). The response (5.48% to 200 ppm CO) of the Chem-FET sensors was also slightly decreased but still high when measured again after 2 weeks from initial sensing tests (**Figure S17**). From these results, we demonstrate that the tuning of the electronic structure of Au NPs by using a gate voltage, in order to promote the catalysis of Au NPs for CO adsorption, leads to the improvement of CO sensing properties of SWCNT chemiresistors. The recent studies on CNT-based CO sensors are summarized in Table S1. The responses of P4VP-SWCNT/Au@ITPES are not superior, however, they are able to stably operate even in humid air and meet the safety standards of OSHA in terms of sensing speed and detection limit, whereas other papers are not. Therefore, these results demonstrate that P4VP-SWCNT/Au@ITPES represents a viable CO sensor.

CONCLUSION

In conclusion, we developed SWCNT-based selective CO sensors with voltage-activated sensitivity by using the porous ion exchange polymer to produce composites with small Au NPs. We demonstrated the important role of ITPES, i) suppressing the growth of Au NPs and creating a uniform localization of ultra-small (< 5 nm) Au NPs on the P4VP-SWCNT and ii) maintaining high gas accessibility within the SWCNT sensing layer. The strong CO adsorption on Au NPs enables sensitive detection of this toxic gas. We further demonstrated that the application of a negative gate voltage in Chem-FET sensors fabricated with P4VP-SWCNT/Au@ITPES as a channel layer promotes the CO adsorption on Au NPs and an improved sensitivity to CO at room temperature in air. The concept of using porous ion exchange polymers for the synthesis of nanoscale metal catalysts-doped SWCNTs can be extended to other kinds of metal NPs.

ASSOCIATED CONTENT

Supporting Information.

Experimental details, ¹H-NMR spectra, SEM/TEM images, profilometer analysis, ATR-FTIR spectra, XPS analysis, charge transfer curves, additional sensing data, and a supporting table. These materials are available free of charge via the Internet at "http://pubs.acs.org."

AUTHOR INFORMATION

Corresponding Author

*E-mail: idkim@kaist.ac.kr. *E-mail: tswager@mit.edu.

ORCID

Yoonseob Kim: 0000-0002-6892-8281 Bora Yoon: 0000-0003-1338-7841 Intak Jeon: 0000-0002-4116-4517 Seon-Jin Choi: 0000-0001-8567-0668 Il-Doo Kim: 0000-0002-9970-2218 Timothy M. Swager: 0000-0002-3577-0510

60

The authors declare no competing financial interest.

ACKNOWLEDGMENT

This work was supported by the National Science Foundation DMR-1809740. This work was also funded by the Ministry of Trade, Industry & Energy (Korea) under Industrial Technology Innovation Program (No. 10070075). This work was also supported by Wearable Platform Materials Technology Center (WMC) funded by National Research Foundation of Korea (NRF) Grant of the Korean Government (MSIP) (No. 2016R1A5A1009926). Y.K. was supported by Abdul Latif Jameel World Water and Food Security Lab (J-WAFS). S.S. was supported by F₃₂ Ruth L. Kirschstein National Research Service Awards. B.Y. was supported by an appointment to the Postgraduate Research Participation Program at CCDC-Soldier Center administered by the Oak Ridge Institute for Science and Education through an interagency agreement between the U.S. Department of Energy and CCDC-Soldier Center.

REFERENCES

- (1) Stetter, J. R.; Li, J., Amperometric Gas Sensors a Review. *Chem. Rev.* **2008**, 108, 352–366.
- (2) Loutfi, A.; Coradeschi, S.; Mani, G. K.; Shankar, P.; Rayappan, J. B. B., Electronic Noses for Food Quality: A Review. *J. Food Eng.* **2015**, *144*, 103–111.
- (3) Guntner, A. T.; Abegg, S.; Konigstein, K.; Gerber, P. A.; Schmidt-Trucksass, A.; Pratsinis, S. E., Breath Sensors for Health Monitoring. *ACS Sens.* **2019**, *4*, 268–280.
- (4) Swager, T. M., Sensor Technologies Empowered by Materials and Molecular Innovations. *Angew. Chem., Int. Ed.* **2018**, 57, 4248–4257.
- (5) Lee, J.-H., Gas Sensors Using Hierarchical and Hollow Oxide Nanostructures: Overview. *Sens. Actuators B* **2009**, 140, 319–336.
- (6) Dey, A., Semiconductor Metal Oxide Gas Sensors: A Review. *Mater. Sci. Eng. B* **2018**, 229, 206–217.
- (7) Schroeder, V.; Savagatrup, S.; He, M.; Lin, S.; Swager, T. M., Carbon Nanotube Chemical Sensors. *Chem. Rev.* **2018**, *119*, 599–663.
- (8) Zanolli, Z.; Leghrib, R.; Felten, A.; Pireaux, J.-J.; Llobet, E.; Charlier, J.-C., Gas Sensing with Au-Decorated Carbon Nanotubes. *ACS Nano* **2011**, 5, 4592–4599.
- (9) Kauffman, D. R.; Star, A., Chemically Induced Potential Barriers at the Carbon Nanotube–Metal Nanoparticle Interface. *Nano Lett.* **2007**, *7*, 1863–1868.
- (10) Kauffman, D. R.; Sorescu, D. C.; Schofield, D. P.; Allen, B. L.; Jordan, K. D.; Star, A., Understanding the Sensor Response of Metal-Decorated Carbon Nanotubes. *Nano Lett.* **2010**, *10*, 958–963.
- (11) Burda, C.; Chen, X.; Narayanan, R.; El-Sayed, M. A., Chemistry and Properties of Nanocrystals of Different Shapes. *Chem. Rev.* **2005**, *105*, 1025–1102.
- (12) Xia, Y.; Xiong, Y.; Lim, B.; Skrabalak, S. E., Shape-Controlled Synthesis of Metal Nanocrystals: Simple Chemistry Meets Complex Physics? *Angew. Chem., Int. Ed.* **2009**, 48, 60–103.
- (13) Li, X.; Le Thai, M.; Dutta, R. K.; Qiao, S.; Chandran, G. T.; Penner, R. M., Sub-6 nm Palladium Nanoparticles for Faster, More Sensitive H₂ Detection Using Carbon Nanotube Ropes. *ACS Sens.* **2017**, *2*, 282–289.
- (14) Choi, S.-W.; Kim, J.; Lee, J.-H.; Byun, Y. T., Remarkable Improvement of CO-Sensing Performances in Single-Walled Carbon Nanotubes due to Modification of the Conducting Channel by Functionalization of Au Nanoparticles. *Sens. Actuators B* **2016**, 232, 625–632.
- (15) Hotze, E. M.; Phenrat, T.; Lowry, G. V., Nanoparticle Aggregation: Challenges to Understanding Transport and

- Reactivity in the Environment. J. Environ. Qual. 2010, 39, 1909–1024.
- (16) Polte, J., Fundamental Growth Principles of Colloidal Metal Nanoparticles—A New Perspective. *CrystEngComm* **2015**, *17*, 6809–6830.
- (17) Kim, Y.; Moh, L. C.; Swager, T. M., Anion Exchange Membranes: Enhancement by Addition of Unfunctionalized Triptycene Poly(Ether Sulfone)s. *ACS Appl. Mater. Interfaces* **2017**, *9*, 42409–42414.
- (18) Xu, T., Ion Exchange Membranes: State of Their Development and Perspective. *J. Membr. Sci.* **2005**, 263, 1–29.
- (19) Rifai, S.; Breen, C. A.; Solis, D. J.; Swager, T. M., Facile in Situ Silver Nanoparticle Formation in Insulating Porous Polymer Matrices. *Chem. Mater.* **2006**, *18*, 21–25.
- (20) Eustis, S.; El-Sayed, M. A., Why Gold Nanoparticles Are More Precious than Pretty Gold: Noble Metal Surface Plasmon Resonance and Its Enhancement of the Radiative and Nonradiative Properties of Nanocrystals of Different Shapes. *Chem. Soc. Rev.* 2006, 35, 209–217.
- (21) Saha, K.; Agasti, S. S.; Kim, C.; Li, X.; Rotello, V. M., Gold Nanoparticles in Chemical and Biological Sensing. *Chem. Rev.* **2012**, *112*, 2739–2779.
- (22) Lemire, C.; Meyer, R.; Shaikhutdinov, S.; Freund, H. J., Do Quantum Size Effects Control CO Adsorption on Gold Nanoparticles? *Angew. Chem., Int. Ed.* **2004**, *43*, 118–121.
- (23) Yoon, B.; Liu, S. F.; Swager, T. M., Surface-Anchored Poly(4-vinylpyridine)–Single-Walled Carbon Nanotube–Metal Composites for Gas Detection. *Chem. Mater.* **2016**, *28*, 5916–5924.
- (24) Tsui, N. T.; Paraskos, A. J.; Torun, L.; Swager, T. M.; Thomas, E. L., Minimization of Internal Molecular Free Volume: A Mechanism for the Simultaneous Enhancement of Polymer Stiffness, Strength, and Ductility. *Macromolecules* **2006**, *39*, 3350–3358.
- (25) McGhee, L.; Siddique, R. M.; Winfield, J. M., Reactions of Hexakis(acetonitrile)iron(II) Hexafluorophosphate in Acetonitrile. Ligation of Ammonia, Pyridine, and Trimethylamine to Iron(II) and the Behaviour of Trimethyl Phosphite and Trimethylphosphine towards Iron(II), Nitrogen Donor Ligand Complex Cations. *J. Chem. Soc., Dalton Trans.* 1988, 1309–1314.
- (26) Link, S.; El-Sayed, M. A., Size and Temperature Dependence of the Plasmon Absorption of Colloidal Gold Nanoparticles. *J. Phys. Chem. B* **1999**, 103, 4212–4217.
- (27) Long, T. M.; Swager, T. M., Molecular Design of Free Volume as a Route to Low-κ Dielectric Materials. *J. Am. Chem. Soc.* **2003**, *12*5, 14113–14119.
- (28) Willets, K. A.; Van Duyne, R. P., Localized Surface Plasmon Resonance Spectroscopy and Sensing. *Annu. Rev. Phys. Chem.* **2007**, 58, 267–297.
- (29) Koo, W. T.; Cha, J. H.; Jung, J. W.; Choi, S. J.; Jang, J. S.; Kim, D. H.; Kim, I. D., Few-Layered WS₂ Nanoplates Confined in Co, N-Doped Hollow Carbon Nanocages: Abundant WS₂ Edges for Highly Sensitive Gas Sensors. *Adv. Funct. Mater.* **2018**, 28, 1802575.
- (30) Thomason, M. J.; Seabourne, C.; Sattelle, B. M.; Hembury, G. A.; Stevens, J.; Scott, A.; Aziz, E. F.; Schroeder, S. L., Self-Association of Organic Solutes in Solution: a NEXAFS Study of Aqueous imidazole. *Faraday Discuss.* **2015**, *179*, 269–289.
- (31) Joo, S. H.; Pak, C.; Kim, E. A.; Lee, Y. H.; Chang, H.; Seung, D.; Choi, Y. S.; Park, J.-B.; Kim, T. K., Functionalized Carbon Nanotube-Poly(Arylene Sulfone) Composite Membranes for Direct Methanol Fuel Cells with Enhanced Performance. *J. Power Sources* **2008**, *18*0, 63–70.
- (32) Luo, J.; Liu, Y.; Niu, Y.; Jiang, Q.; Huang, R.; Zhang, B.; Su, D., Insight into the Chemical Adsorption Properties of CO Molecules Supported on Au or Cu and Hybridized Au–CuO Nanoparticles. *Nanoscale* **2017**, *9*, 15033–15043.
- (33) Figueiredo, N.; Carvalho, N.; Cavaleiro, A., An XPS Study of Au Alloyed Al–O Sputtered Coatings. *Appl. Sur. Sci.* **2011**, 257, 5793–5798.

- (34) Charlier, J.-C.; Arnaud, L.; Avilov, I.; Delgado, M.; Demoisson, F.; Espinosa, E.; Ewels, C. P.; Felten, A.; Guillot, J.; Ionescu, R., Carbon Nanotubes Randomly Decorated with Gold Clusters: From Nano2hybrid Atomic Structures to Gas Sensing Prototypes. *Nanotechnology* 2009, 20, 375501.
- (35) Li, J.; Lu, Y.; Ye, Q.; Cinke, M.; Han, J.; Meyyappan, M. Carbon Nanotube Sensors for Gas and Organic Vapor Detection. *Nano Lett.* **2003**, *3*, 929–933.
- (36) Carbon Monoxide In Workplace Atmospheres (Direct-Reading Monitor), OSHA Method ID-209; Occupational Safety and Health Administration, 1993.
- (37) Widmann, D.; Behm, R. J., Active Oxygen on a Au/TiO_2 Catalyst: Formation, Stability, and CO Oxidation Activity. *Angew. Chem., Int. Ed.* **2011**, 50, 10241–10245.
- (38) Mpourmpakis, G.; Andriotis, A. N.; Vlachos, D., Identification of Descriptors for the CO Interaction with Metal Nanoparticles. *Nano Lett.* **2010**, *10*, 1041–1045.
- (39) Ferrari, P.; Vanbuel, J.; Janssens, E.; Lievens, P., Tuning the Reactivity of Small Metal Clusters by Heteroatom Doping. *Acc. Chem. Res.* **2018**, *51*, 3174–3182.
- (40) Lari, G. M.; Nowicka, E.; Morgan, D. J.; Kondrat, S. A.; Hutchings, G. J., The Use of Carbon Monoxide as a Probe Molecule in Spectroscopic Studies for Determination of Exposed

- Gold Sites on TiO₂. *Phys. Chem. Chem. Phys.* **2015**, *17*, 23236–23244.
- (41) Blyholder, G., Molecular Orbital View of Chemisorbed Carbon Monoxide. *J. Phys. Chem.* **1964**, *68*, 2772–2777.
- (42) Barnard, A., Modelling of Nanoparticles: Approaches to Morphology and Evolution. *Rep. Prog. Phys.* **2010**, 73, 086502.
- (43) Wang, S.; Wang, X., Imidazolium Ionic Liquids, Imidazolylidene Heterocyclic Carbenes, and Zeolitic Imidazolate Frameworks for CO₂ Capture and Photochemical Reduction *Angew. Chem., Int. Ed.* **2016**, 55, 2308–2320.
- (44) Savagatrup, S.; Schroeder, V.; He, X.; Lin, S.; He, M.; Yassine, O.; Salama, K. N.; Zhang, X. X.; Swager, T. M., Bio-Inspired Carbon Monoxide Sensors with Voltage-Activated Sensitivity. *Angew. Chem., Int. Ed.* **2017**, *129*, 14254–14258.
- (45) Lin, X.; Yang, B.; Benia, H.-M.; Myrach, P.; Yulikov, M.; Aumer, A.; Brown, M. A.; Sterrer, M.; Bondarchuk, O.; Kieseritzky, E., Charge-Mediated Adsorption Behavior of CO on MgO-Supported Au Clusters. *J. Am. Chem. Soc.* **2010**, *1*32, 7745–7749.
- (46) Wu, X.; Senapati, L.; Nayak, S.; Selloni, A.; Hajaligol, M., A Density Functional Study of Carbon Monoxide Adsorption on Small Cationic, Neutral, and Anionic Gold Clusters. *J. Chem. Phys.* **2002**, *11*7, 4010–4015.

